Coherent optical association of atoms into a single molecule

Yichao Yu,[1,2,3,*] Kenneth Wang,[1,2,3] Jonathan D. Hood,[4] Lewis R. B. Picard,[1,2,3] Jessie T. Zhang,[1,2,3] William B. Cairncross,[2,1,3] Jeremy M. Hutson,[5] Till Rosenband,[1] and Kang-Kuen Ni[2,1,3,†]

[1] *Department of Physics, Harvard University, Cambridge, Massachusetts 02138, USA*
[2] *Department of Chemistry and Chemical Biology, Harvard University, Cambridge, Massachusetts 02138, USA*
[3] *Harvard-MIT Center for Ultracold Atoms, Cambridge, Massachusetts 02138, USA*
[4] *Department of Chemistry, Purdue University, West Lafayette, Indianna, 47906, USA*
[5] *Joint Quantum Centre Durham-Newcastle, Department of Chemistry, Durham University, Durham, DH1 3LE, United Kingdom*

(Dated: November 10, 2020)

Fully controlled single molecules provide a promising platform for a variety of quantum science applications. As a step towards this goal, we report on coherent association of atoms into a single weakly bound NaCs molecule in an optical tweezer through an optical Raman transition without the use of a Feshbach resonance. The Raman scheme uses a deeply bound electronic excited intermediate state to achieve a large transition dipole moment while reducing the photon scattering. Starting from two atoms in their relative motional ground state, we achieve an optical transfer efficiency of 69 %. The molecule has a binding energy of 770.20052(2) MHz at 8.8 G and are created with higher than 60 % probability in the motional ground state. This technique does not rely on narrow excited-state lines or Feshbach resonances and will allow a wider range of molecular species to be assembled atom-by-atom.

Diverse species of fully quantum controlled ultracold molecules are desired for a wide variety of applications including precision measurements [1–6], quantum simulations [7–10], quantum information processing [11–14], and studies of ultracold chemistry [15–18]. While many innovative approaches demonstrated in the last few years have directly cooled different species of diatomic or polyatomic molecules below 1 mK [19–24], the highest phase-space-density gas [25] and the coldest individual molecules [26, 27] have been achieved through the association of ultracold atoms.

Molecular association of ultracold atoms takes advantage of the cooling and trapping techniques that have been developed for atoms. Associating atoms into deeply-bound molecules is challenging because of the small wavefunction overlap between the free-atom and molecular states and the release of a large amount of binding energy. A two-step approach has been demonstrated to associate atom pairs into weakly bound molecules first, and then transfer the molecules from this single internal state to a desired rovibrational and electronic state, releasing the binding energy by stimulated emission [1, 28–35]. So far, most molecular association has been achieved for bialkali molecules by magnetoassociation using a magnetic Feshbach scattering resonance. The only exceptions are Sr_2, where narrow linewidth ($\sim$ 20 kHz) excited states are available and optical association can be driven coherently [36, 37], and ^{87}Rb^{85}Rb, where there are molecular states bound by $1 \sim 2$ MHz [27]. With these requirements, molecules involving non-magnetic atoms or atoms without narrow intercombination lines remain difficult to associate.

Here, we demonstrate coherent association of an atom pair to a weakly bound molecule using a two-photon optical Raman transfer via an electronic excited state, schematically shown in Fig. 1a. The scheme does not rely on a Feshbach resonance, molecular states bound by a few MHz, or a narrow excited state. The resulting single molecule is in a well-defined internal quantum state and predominantly in its motional ground state. A vibrational state of the electronic excited state $c^3\Sigma^+(\Omega = 1)$ is used as the intermediate state in the Raman scheme, and is chosen to minimize the theoretical photon scattering during a Raman Rabi oscillation. To reduce the photon scattering and sensitivity to laser intensity noise further, we choose the initial and final state to balance the two Rabi frequencies as much as possible. This system-independent approach can be used for creating new molecules atom-by-atom with full quantum state control.

The essence of an optical Raman transfer can be illustrated using a three-level system shown in Fig. 1a, where the initial atomic state and the target weakly bound molecular state are coupled to an intermediate state by two lasers with Rabi frequencies, Ω_a and Ω_m, with one-photon detuning Δ, and two-photon detuning, δ. The transfer Raman Rabi Rate, $\Omega_a\Omega_m/2\Delta$, is accompanied by a photon scattering rate $\Gamma_e(\Omega_a^2 + \Omega_m^2)/4\Delta^2$ [38]. Unlike Raman transitions in atoms, the two Rabi frequencies are greatly imbalanced due to the small wavefunction overlap between the atomic state and the intermediate state, and therefore the scattering is predominantly from the target molecular state. Furthermore, the energy difference between the atomic state and target molecular state is small (< 1 GHz) compared to the single-photon detuning, Δ, so the target molecular state can scatter off both beams roughly equally. Thus, the scattering rate is given by $\Gamma_e\Omega_m^2/2\Delta^2$, where Γ_e is the

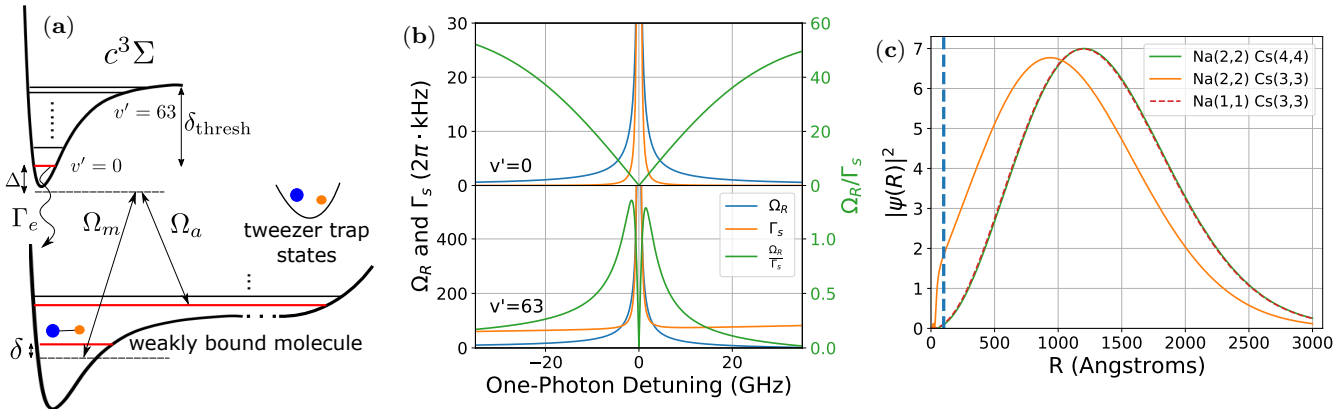

FIG. 1. Optical creation of single molecule from single atoms in tweezer. (a) Schematic of the optical transition from an atom pair to a weakly bound molecule. The initial state is the relative motional ground state between the two atoms and the final state is the first molecular bound state. The transition is driven by a pair of laser frequencies matching the binding energy of the molecule. The lasers are detuned from an excited molecular state in the $c^3\Sigma$ potential by Δ in order to suppress the scattering during the transfer. (b) Comparison between using a weakly bound and a deeply bound excited state as intermediate state for the Raman transition. The deeply bound excited state (upper half $v' = 0$) has a smaller Raman Rabi frequency (Ω_R) compared to the weakly bound excited state (lower half $v' = 63$) at a given detuning. However, the scattering rate (Γ_s) is also much lower, which results in a larger Raman Rabi frequency to scattering rate ratio. (c) Enhancement of the short-range wavefunction. The large scattering length for the $\text{Na}(2,2), \text{Cs}(3,3)$ state creates an interaction shift comparable to the axial trapping frequency. This causes a significant change in the relative wavefunction especially at short intranuclear distance (R). Compared to other spin states with weaker interaction, the wavefunction at short distance ($R < 100$Å, left of the dotted line) is significantly enhanced.

excited-state linewidth [39]. The ratio between the Raman Rabi frequency and the scattering rate is therefore $\Omega_a/\Omega_m \times \Delta/\Gamma_e$. To ensure a coherent process, a detuning as large as possible, while maintaining a realistic Raman Rabi frequency, is preferred.

Early experiments used weakly bound excited states as the intermediate state in the Raman transition to ensure a large Raman Rabi frequency [40, 41]. However, a complete picture must include both the many vibrational levels of the excited electronic state and the atomic continuum. The total scattering rate and Raman Rabi rate become a sum of the scattering rates and Raman Rabi rates over all possible intermediate states. With these considerations, using a weakly bound excited state as the intermediate state suffers from strong scattering due to the nearby excited atomic continuum, resulting in large incoherence and loss to other molecular states. This scattering is proportional to $1/\delta_{\text{thresh}}^2$, where δ_{thresh} is the detuning from the dissociation threshold, and thus can be made smaller by using deeply bound vibrational states as the intermediate level.

To find the optimal intermediate state, we perform a calculation of the Raman Rabi frequency Ω_R and scattering rate Γ_s at different detunings from the atomic threshold taking into account of all states of the $c^3\Sigma^+(\Omega = 1)$ excited molecular state potential [42] and the continuum [43]. The excited atomic continuum is particularly important for the target molecular state. The sum of the squares of the wavefunction overlap between the target weakly bound molecular state and all the excited molecular bound states is only about 0.02, suggesting that there are significant matrix elements between the target molecular state and the excited atomic continuum. This calculation shows that the ratio of the Raman Rabi rate to scattering rate can be made larger for more deeply bound states compared to weakly bound states at a cost of a smaller Raman Rabi frequency, as shown in Fig. 1b; see Supplementary Material for details. As a result, we choose the $v' = 0$ level of $c^3\Sigma^+(\Omega = 1)$ as an intermediate state to drive the Raman transition.

In addition to the intermediate state, choosing an initial and a final state for a large ratio Ω_a/Ω_m maximizes the Raman Rabi frequency at a given detuning. Furthermore, a larger ratio also relaxes the intensity stability requirement, because this is also the ratio between the Raman Rabi coupling and the AC Stark shift of the molecular state, $\Omega_m^2/2\Delta$ [44]. Due to the small extent of the intermediate-state wavefunction compared to that of the trapped atoms, Ω_a is approximately proportional to the amplitude of the relative atomic wavefunction at short distance, within the range of the molecular potential. To increase this amplitude, one can increase the external confinement of atom pairs. Using a harmonic approximation, the short-range amplitude is proportional to $\omega_{\text{trap}}^{3/4}$ or $P^{3/8}$, where ω_{trap} is the trap frequency and P is the power in the trap [45]. However, additional power may not always be available, and will also lead to additional undesired scattering. Alternatively, one can choose

an atomic pair state with a large scattering length (positive or negative). For such states, the amplitude of the relative atomic wavefunction is substantially enhanced at short range, as shown in Fig. 1c. For our system of Na and Cs atoms, we choose a spin-state combination $|\uparrow_{\rm Na}\downarrow_{\rm Cs}\rangle \equiv |F=2,m_F=2\rangle_{\rm Na}|F=3,m_F=3\rangle_{\rm Cs}$ that has a large and negative scattering length of $a(\uparrow_{\rm Na}\downarrow_{\rm Cs}) \approx -700a_0$ [46]. All other stable spin combinations give smaller scattering lengths ($< 50\ a_0$). For the target molecular state, the spin state is ideally similar to the initial spin state in order to minimize sensitivity to the magnetic field. Coupled-channel calculations show that this target molecular state with similar spin composition also has reduced Rabi frequency, Ω_m, with the intermediate state when compared to bound states of the other spin compositions. This further increases the ratio Ω_a/Ω_m when using the $|\uparrow_{\rm Na}\downarrow_{\rm Cs}\rangle$ hyperfine combination. This combination results in a ratio Ω_a/Ω_m of about 0.05 instead of a ratio of about 0.003 with the other combinations, thus relaxing the intensity stability requirement to the few percent level.

Experimentally, we first prepare two atoms in a well-defined external and internal quantum state using techniques developed previously [47–49]. In brief, the experimental cycle begins by stochastically loading a single ^{23}Na atom and a single ^{133}Cs atom into separate optical tweezers. The atoms are initially imaged to distinguish between loading of two atoms, one atom (Na or Cs), or no atom to be able to post-select from the experimental results based on the initial loading condition. Raman sideband cooling is then applied to prepare both atoms simultaneously in the 3-dimensional motional ground state of their optical tweezers. After cooling, the Na and Cs atoms are in the spin state $|\uparrow_{\rm Na}\uparrow_{\rm Cs}\rangle \equiv |F=2,m_F=2\rangle_{\rm Na}|F=4,m_F=4\rangle_{\rm Cs}$, which has a small scattering length. The weak two-atom interaction allows the merging of the two tweezers to be done with minimum pertubation so that they remain in the motional ground state.

Next, we drive the atoms into spin combination $|\uparrow_{\rm Na}\downarrow_{\rm Cs}\rangle$, which has large scattering length, by performing a Cs spin flip while taking into account the -30.7 kHz interaction shift [46]. We use this as the initial atomic state for Raman transfer. This spin flip selectively transfers atoms in the relative motional ground state, removing any background from atoms in excited motional states [50]. For the experiment reported here, 31 % of our initial two-atom population is transferred.

To perform the Raman transfer of an atom pair to the target weakly bound molecular state, we use the tweezer beam itself as the Raman beams by turning on two frequencies in the tweezer during the Raman pulse, as shown in Fig. 2b inset. The dual use of the tweezer beam not only eliminates additional scattering sources or undesired laser frequencies, but also allows a tight focus to maximize the Raman Rabi frequency and minimize

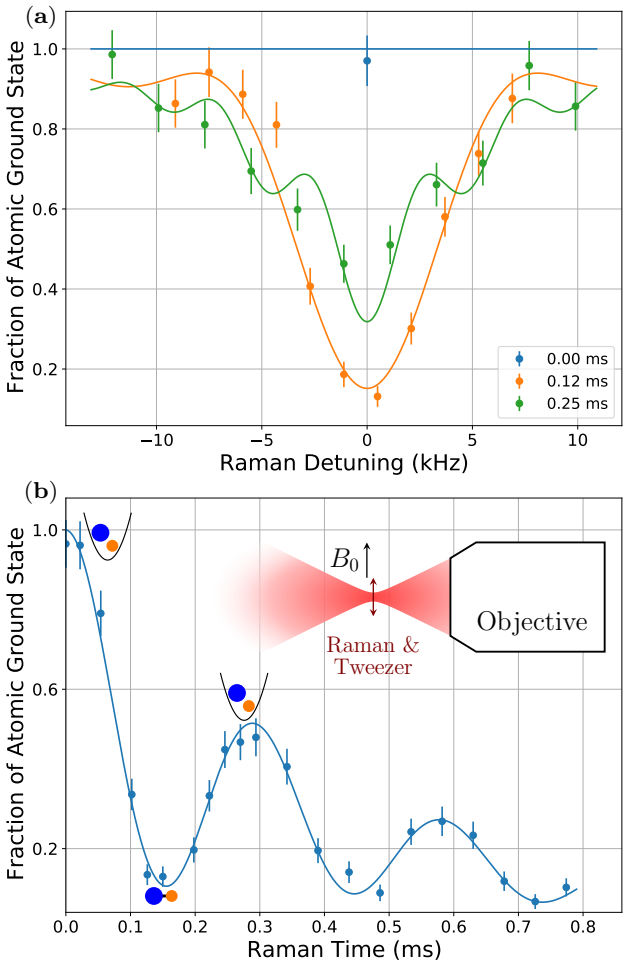

FIG. 2. (a) Raman detuning scans at different times showing the resonance frequency. (b) Raman pulse time scan on resonance. A decaying Rabi oscillation can be observed proving the coherence of the Raman transfer process. This is fitted together with (a) to a model of the Raman transition including loss of the atom and molecule state and is used to determine both the Raman Rabi frequency and the loss rates. Inset: Geometry and polarization of trap and Raman beam relative to the bias magnetic field. The tweezer and Raman beam is focused through an objective to a waist of 0.9 μm which defines the location of the atoms and molecule. We use a bias B field of $B_0 = 8.8$ G along the tweezer polarization to define the quantization axis. As a result, the atoms experiences predominantly π polarization from the tweezer.

the transfer time. Furthermore, we use a Bragg grating with a linewidth (FWHM) of 50 GHz to filter the laser spectrum generated by a fiber amplifier that is seeded with a 1037 nm external cavity diode laser. We observe a reduction of the scattering rate by a factor of 2 due to suppression of the broadband amplified spontaneous emission (ASE) from the laser that couples to other excited states. After the total tweezer power is set to the desired value, we smoothly ramp down the power of one frequency in the tweezer while simultaneously ramping

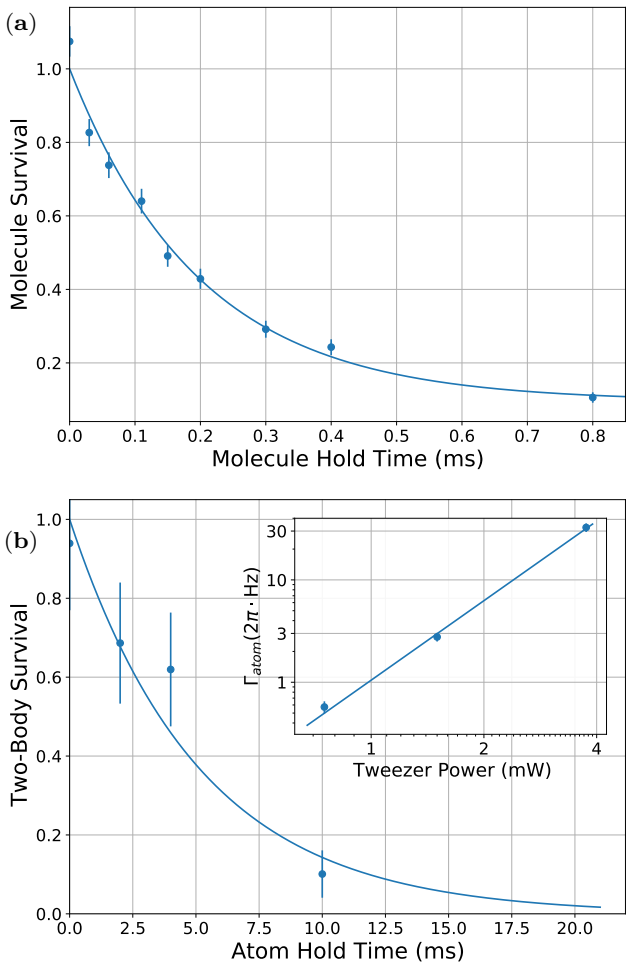

FIG. 3. (a) Direct measurement of molecule lifetime in 3.75 mW of trap depth. Molecule survival is detected by dissociating back to atoms using a second Raman transition. The lifetime is consistent with the 0.199(9) ms measured from the Raman transition data. (b) Two-body atom lifetime of 5(1) ms in 3.75 mW of trap depth caused by off-resonance photoassociation. This is used to improve the fitting of the Raman transfer data. Inset: Atomic scattering rate scales as $P_{tweezer}^{2.58}$ on a log-log scale, this is consistent with a two-photon scattering process. We have not measured a clear dependency of the loss rate on the tweezer detuning.

up the power of a different frequency so that the total tweezer power remains unchanged. Both frequencies are kept on for a specified duration before the process is reversed and the tweezer returns to a single frequency.

We choose the tweezer frequency to be far detuned (by 145 GHz) from the $v' = 0$ line. Guided by coupled-channel calculations, we locate the Raman resonance for the atoms-to-molecule transition at 770.57150(9) MHz with 3.75 mW tweezer power, as shown in Fig. 2a. The molecular state is dark to the imaging step, so successful transfer of the atoms to the molecular state is detected as loss. We observe a fourier-limited linewidth, which is evidence of a coherent transfer. In order to verify the coherence of the transfer directly, we fix the two-photon detuning on resonance and scan the pulse time. Fig. 2b shows the observed coherent Rabi oscillation between the atomic and molecular states. Fitting the data with a decaying Rabi oscillation suggests that 69 % of atoms initially in the motional ground state are transferred into the molecular state after a π pulse. This transfer efficiency is limited mainly by the molecular lifetime, which can be measured directly by preparing the molecule with a π pulse and then using a second π pulse to dissociate the molecule back to atoms after a variable wait time. The result in Fig. 3a shows a molecular lifetime of 0.199(9) ms consistent with the decay of Rabi oscillation. We obtain the Raman Rabi frequency by fitting our measurements to a model that includes a Raman Rabi frequency and a finite lifetime for the molecular state, as shown in Fig. 2a and b. We account for the effect of atomic state loss by measuring the one-body and two-body lifetime of the atoms directly without turning on the second frequency, as shown in Fig. 3b. The fit gives a Raman Rabi frequency of $2\pi \times 3.28(4)$ kHz.

The efficiency of the transfer is lower than expected because the ratio of the molecular scattering rate to the Rabi frequency is 10 times larger than predicted. Based on the discussion above, if this discrepancy arises from the $v' = 0$ excited state, it can be due either to a high ratio Ω_m/Ω_a or to a large Γ_e. Additionally, coupling to other excited states can add an offset to both the Raman Rabi frequency and the scattering rate and thus affect their ratio.

In order to verify whether any one of these known sources are the origin of the discrepancy, we measured the properties of the Raman resonance as a function of the tweezer power and single-photon detuning. These dependencies allow us to experimentally determine the matrix elements, Ω_a, Ω_m and how much of the scattering, Stark shift, or Raman Rabi frequency comes from the $v' = 0$ intermediate state.

First we look at the change in resonance frequency. As a function of the tweezer power, we observe the expected linear dependency on the resonance frequency caused by the differential light shift between the atomic and molecular state. When we vary the tweezer frequency around the $v' = 0$ intermediate state, we can further observe a $1/\Delta$ component and a constant background in the experimentally explored region, as shown in Fig. 4a. The background is caused by coupling to other excited states that are further away in energy. The $1/\Delta$ component, however, is due to the coupling between the molecular state and the $v' = 0$ intermediate state. From this measurement, we can extract a Ω_m of $2\pi \times 72.32(4)$ MHz/$\sqrt{\text{mW}}$ or $2\pi \times 140.06(8)$ MHz for the 3.75 mW tweezer power used above. This number is close to the value of $2\pi \times 40.7$ MHz/$\sqrt{\text{mW}}$ calculated from theory.

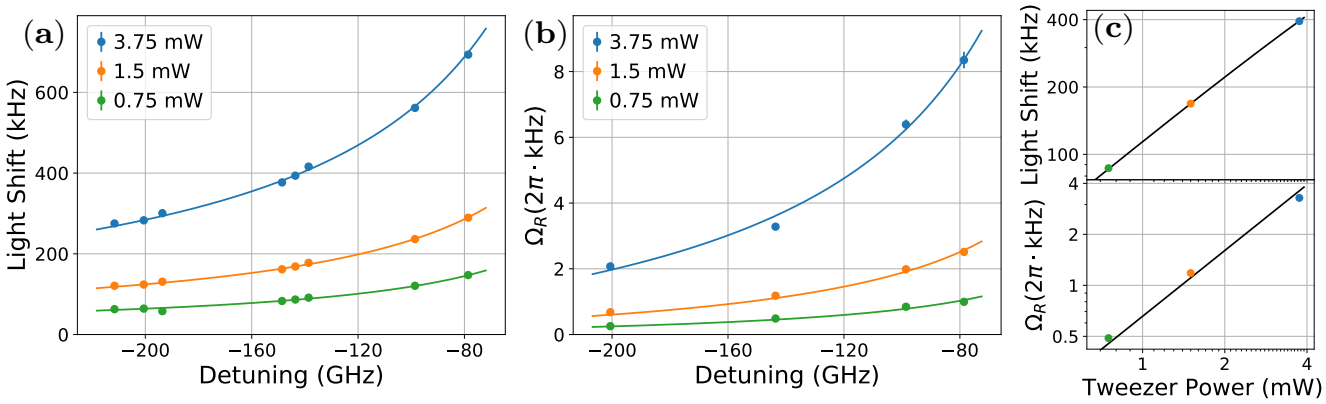

FIG. 4. Raman transition parameters as a function of tweezer and Raman power and detuning. The detuning is calculated from the closest $v' = 0$ PA frequency at 288703.6 GHz. (a) The light shift of the Raman resonance scales as P and follows $1/\Delta$ with an offset, where P is the power in the tweezer. The fit also includes a small term that is proportional to P^2 which is caused by the effective magnetic field generated by the tweezer which is perpendicular to the real magnetic field. (b) Raman Rabi frequency (Ω_R) scales as $P^{1.29}$ and follows $1/\Delta$ with an offset. (c) Tweezer power dependency of light shift (up) and Raman Rabi frequency (down) on a log-log plot showing the power law scaling.

In order to calculate the ratio Ω_m/Ω_a, we now need to extract Ω_a. We do this by measuring the dependencies of the Raman Rabi frequency, which depends on both Ω_m and Ω_a. The Raman Rabi frequency shows a non-linear dependency on the tweezer power due to the change in the atomic wavefunction caused by tighter confinement at higher power, as shown in Fig. 4b. As discussed before, for weakly interacting particles, Ω_a scales as $P^{0.375}$. However, due to the strong interaction between the two atoms, this approximation breaks down. Instead, coupled-channel calculations show that the scaling is very well approximated by $P^{0.29}$ within the range of confinement in our experiment. Combined with the standard intensity factor, the Raman Rabi frequency should scale as $P^{1.29}$, which fits well to our experimental result, as shown in Fig. 4c. Similar to the light shift, the detuning dependency of the Raman Rabi frequency is determined by a constant background component and a $v' = 0$ component that scales as $1/\Delta$. The $v' = 0$ component of the Raman Rabi frequency is $2\pi \times 1.02(2)$ kHz $\cdot$ mW$^{-1.29}$, or $2\pi \times 5.6(1)$ kHz at 3.75 mW tweezer power. Together with the Ω_m measured above, the Rabi frequency, Ω_a, is $2\pi \times 12.1(3)$ MHz. This gives a matrix-element ratio of 11.6(3), which is in fact better than the theory prediction of 23.8 (Table I). Therefore, this should not cause the ratio of the Raman Rabi frequency to scattering rate from the $v' = 0$ state to be higher than expected. Furthermore, we independently measure the natural linewidth of the $v' = 0$ excited state to be no larger than 20 MHz using photoassociation (PA) spectroscopy. This suggests that the excited-state linewidth should not cause a stronger than expected scattering from $v' = 0$ state either.

With the $v' = 0$ state ruled out as the source of discrepancy between experiment and theory, we now consider the background effects from other states with larger single-photon detuning. In the Raman Rabi frequency fit, the fitted background is of opposite sign from the Raman Rabi frequency for single-photon detunings red of the $v' = 0$ transition. Thus, this background reduces the Raman Rabi frequency by about 30 % at the current detuning. However, this difference is not enough to explain the discrepancy of more than a factor of 10 present in the experiment. Due to the change in sign of the Raman Rabi frequency as a function of detuning when crossing a resonance, the same background will increase the Raman Rabi frequency for positive detunings from the $v' = 0$ transition, which increases the Raman Rabi frequency. Unfortunately, we observe additional nearby excited states belonging to a different electronically excited state at higher frequencies which prevent the blue side of the transition to be usable for the Raman transition.

These results suggest that the decoherence or loss we observe during the Raman transition comes from either a higher than expected background scattering rate or a different intrinsic or technical source that we have not accounted for. We observe a decrease in the coherence time by a factor of 2 without the ASE filter, suggesting the spectral purity of the laser is a significant source of

	Experiment	Theory
Ω_m	$2\pi \times 140.06(8)$ MHz	$2\pi \times 78.9$ MHz
Ω_a	$2\pi \times 12.1(3)$ MHz	$2\pi \times 3.32$ MHz
Ω_m/Ω_a	11.6(3)	23.8

TABLE I. Comparison between theory and experiment of the Rabi frequencies Ω_m and Ω_a at 3.75 mW tweezer power. The experimentally measured ratio Ω_m/Ω_a is smaller than the theory prediction.

scattering. Other sources that can contribute to the decoherence include the stability of the tweezer power and the magnetic field. Based on the ratio of the Raman Rabi frequency to light shift, shown in Fig. 4c, the requirement on the tweezer power stability is 0.8 % at 3.75 mW, which we stabilize to 0.1 % so this should not be a major source of decoherence. Similarly, we measured a Zeeman shift of 42.2(2) kHz/G which does not cause significant decoherence from the measured magnetic field fluctuation of ~ 1.5 mG.

The scattering rate of the molecule also depends on the tweezer power and detuning, and becomes smaller when the power is lowered. At 0.75 mW tweezer power, we observe a molecule lifetime as long as 1 ms. However, since the technical noise that can lead to decoherence is not fully characterized in our experiment, we are unable to further identify the sources of the measured scattering rate based on our measured detuning and power dependencies.

Lastly, to confirm that the excess scattering does not come from the atomic state, we measure the two-body scattering rate without turning on the second frequency, as shown in Fig. 3b inset. The scattering rate scales as $P_{\text{tweezer}}^{2.58}$, which is inconsistent with a single-photon scattering process. We have not been able to observe a dependency on the detuning in order to verify if the scattering process is related to the $v' = 0$ state, but the power scaling strongly suggests the existence of an unknown two-photon process. Nevertheless, the absolute scattering rate from the atomic state is much lower than the total scattering rate and is not the limiting factor in this experiment.

In conclusion, we have formed a weakly bound NaCs molecule in an optical tweezer by optical Raman transfer. A theoretical investigation including all excited states of $c^3\Sigma^+(\Omega = 1)$, the excited atomic continuum, and coupled-channel ground state wavefunctions indicated better transfer efficiency using a deeply bound intermediate state and the $|\uparrow_{\text{Na}}\downarrow_{\text{Cs}}\rangle$ spin state as the initial and final states. Using these theoretical insights, we located the weakly bound state and coherently associated the atoms into a weakly bound molecule. Our transfer efficiency is limited by an unknown scattering source resulting in measured scattering rates over 10 times larger than theoretical predictions. Despite this limitation, the transfer efficiency may be further improved by increasing the ratio of the up-leg to down-leg Rabi frequency Ω_a/Ω_m, for example by driving to more deeply bound states. There may also be a better choice of single-photon detuning to increase the Raman Rabi frequency, since our location results in about 30 % cancellation of the Raman Rabi frequency due to an offset of unknown origin.

Our technique can be applied to form a more diverse set of molecular species, since it does not rely on a magnetic Feshbach resonance, states bound by a few MHz, or a narrow excited state. The formation of a weakly bound molecule is a key step in forming rovibrational ground state molecules. Combined with real-time rearrangement [51, 52], defect-free arrays of highly controlled molecules comprise a promising and flexible platform for quantum simulation and quantum computing applications.

We would like to thank Bo Gao, Paul Julienne, and Rosario Gonzalez-Ferez for discussion. This work is supported by the NSF (PHY-1806595), the AFOSR (FA9550-19-1-0089), ARO DURIP (W911NF1810194) and the Arnold and Mabel Beckman foundation. J. T. Z. is supported by a National Defense Science and Engineering Graduate Fellowship. W. C. is supported by a Max Planck-Harvard Research Center for Quantum Optics fellowship. K. W. is supported by an NSF GRFP fellowship. J. M. H. is supported by the U.K. Engineering and Physical Sciences Research Council (EPSRC) Grants No. EP/N007085/1, EP/P008275/1 and EP/P01058X/1.

* yichaoyu@g.harvard.edu
† ni@chemistry.harvard.edu

[1] S. S. Kondov, C.-H. Lee, K. H. Leung, C. Liedl, I. Majewska, R. Moszynski, and T. Zelevinsky, Nature Physics **15**, 1118–1122 (2019).
[2] I. Kozyryev and N. R. Hutzler, Physical Review Letters **119**, 133002 (2017), publisher: American Physical Society.
[3] V. V. Flambaum and V. A. Dzuba, Phys. Rev. A **101**, 042504 (2020).
[4] V. Andreev, D. G. Ang, D. DeMille, J. M. Doyle, G. Gabrielse, J. Haefner, N. R. Hutzler, Z. Lasner, C. Meisenhelder, B. R. O'Leary, C. D. Panda, A. D. West, E. P. West, X. Wu, and A. C. M. E. Collaboration, Nature **562**, 355 (2018).
[5] W. B. Cairncross, D. N. Gresh, M. Grau, K. C. Cossel, T. S. Roussy, Y. Ni, Y. Zhou, J. Ye, and E. A. Cornell, Phys. Rev. Lett. **119**, 153001 (2017).
[6] J. J. Hudson, D. M. Kara, I. J. Smallman, B. E. Sauer, M. R. Tarbutt, and E. A. Hinds, Nature **473**, 493 (2011).
[7] A. Micheli, G. Brennen, and P. Zoller, Nat. Phys. **2**, 341 (2006).
[8] N. Y. Yao, M. P. Zaletel, D. M. Stamper-Kurn, and A. Vishwanath, Nature Physics **14**, 405 (2018).
[9] M. L. Wall, K. R. A. Hazzard, and A. M. Rey, From atomic to mesoscale: The role of quantum coherence in systems of various complexities (World Scientific, 2015) Chap. Quantum magnetism with ultracold molecules.
[10] M. Wall, K. Maeda, and L. D. Carr, New Journal of Physics **17**, 025001 (2015).
[11] D. DeMille, Phys. Rev. Lett. **88**, 067901 (2002).
[12] K.-K. Ni, T. Rosenband, and D. D. Grimes, Chem. Sci. **9**, 6830 (2018).
[13] E. R. Hudson and W. C. Campbell, Phys. Rev. A **98**, 040302(R) (2018).
[14] Y. Lin, D. R. Leibrandt, D. Leibfried, and C.-W. Chou, Nature **581**, 273 (2020).
[15] N. Balakrishnan, J. Chem. Phys. **145**, 150901 (2016).

[16] M.-G. Hu, Y. Liu, D. D. Grimes, Y.-W. Lin, A. H. Gheorghe, R. Vexiau, N. Bouloufa-Maafa, O. Dulieu, T. Rosenband, and K.-K. Ni, Science **366**, 1111 (2019).

[17] Y. Segev, M. Pitzer, M. Karpov, N. Akerman, J. Narevicius, and E. Narevicius, Nature **572**, 189 (2019).

[18] T. de Jongh, M. Besemer, Q. Shuai, T. Karman, A. van der Avoird, G. C. Groenenboom, and S. Y. T. van de Meerakker, Science **368**, 626 (2020), https://science.sciencemag.org/content/368/6491/626.full.pdf.

[19] E. B. Norrgard, D. J. McCarron, M. H. Steinecker, M. R. Tarbutt, and D. DeMille, Phys. Rev. Lett. **116**, 063004 (2016).

[20] L. Anderegg, B. L. Augenbraun, Y. Bao, S. Burchesky, L. W. Cheuk, W. Ketterle, and J. M. Doyle, Nature Physics **14**, 890 (2018).

[21] D. Mitra, N. B. Vilas, C. Hallas, L. Anderegg, B. L. Augenbraun, L. Baum, C. Miller, S. Raval, and J. M. Doyle, Science **369**, 1366 (2020).

[22] S. Ding, Y. Wu, I. A. Finneran, J. J. Burau, and J. Ye, Phys. Rev. X **10**, 021049 (2020).

[23] D. J. McCarron, M. H. Steinecker, Y. Zhu, and D. DeMille, Phys. Rev. Lett. **121**, 013202 (2018).

[24] S. Truppe, H. J. Williams, M. Hambach, L. Caldwell, N. J. Fitch, E. A. Hinds, B. E. Sauer, and M. R. Tarbutt, Nature Physics **13**, 1173 (2017).

[25] L. De Marco, G. Valtolina, K. Matsuda, W. G. Tobias, J. P. Covey, and J. Ye, Science **363**, 853 (2019).

[26] J. T. Zhang, Y. Yu, W. B. Cairncross, K. Wang, L. R. B. Picard, J. D. Hood, Y.-W. Lin, J. M. Hutson, and K.-K. Ni, Phys. Rev. Lett. **124**, 253401 (2020).

[27] X. He, K. Wang, J. Zhuang, P. Xu, X. Gao, R. Guo, C. Sheng, M. Liu, J. Wang, J. Li, G. V. Shlyapnikov, and M. Zhan, Science **370**, 331 (2020).

[28] J. G. Danzl, E. Haller, M. Gustavsson, M. J. Mark, R. Hart, N. Bouloufa, O. Dulieu, H. Ritsch, and H.-C. Nägerl, Science **321**, 1062 (2008).

[29] K.-K. Ni, S. Ospelkaus, M. H. G. de Miranda, A. Pe'er, B. Neyenhuis, J. J. Zirbel, S. Kotochigova, P. S. Julienne, D. S. Jin, and J. Ye, Science **322**, 231 (2008).

[30] F. Lang, K. Winkler, C. Strauss, R. Grimm, and J. Hecker Denschlag, Phys. Rev. Lett. **101**, 133005 (2008).

[31] T. Takekoshi, L. Reichsöllner, A. Schindewolf, J. M. Hutson, C. R. Le Sueur, O. Dulieu, F. Ferlaino, R. Grimm, and H.-C. Nägerl, Phys. Rev. Lett. **113**, 205301 (2014).

[32] P. K. Molony, P. D. Gregory, Z. Ji, B. Lu, M. P. Köppinger, C. R. Le Sueur, C. L. Blackley, J. M. Hutson, and S. L. Cornish, Phys. Rev. Lett. **113**, 255301 (2014).

[33] J. W. Park, S. A. Will, and M. W. Zwierlein, Phys. Rev. Lett. **114**, 205302 (2015).

[34] M. Guo, B. Zhu, B. Lu, X. Ye, F. Wang, R. Vexiau, N. Bouloufa-Maafa, G. Quéméner, O. Dulieu, and D. Wang, Phys. Rev. Lett. **116**, 205303 (2016).

[35] K. K. Voges, P. Gersema, M. Meyer zum Alten Borgloh, T. A. Schulze, T. Hartmann, A. Zenesini, and S. Ospelkaus, Phys. Rev. Lett. **125**, 083401 (2020).

[36] G. Reinaudi, C. B. Osborn, M. McDonald, S. Kotochigova, and T. Zelevinsky, Phys. Rev. Lett. **109**, 115303 (2012).

[37] S. Stellmer, B. Pasquiou, R. Grimm, and F. Schreck, Phys. Rev. Lett. **109**, 115302 (2012).

[38] D. J. Wineland, M. Barrett, J. Britton, J. Chiaverini, B. DeMarco, W. M. Itano, B. Jelenković, C. Langer, D. Leibfried, V. Meyer, T. Rosenband, and T. Schätz, Philosophical Transactions of the Royal Society of London A: Mathematical, Physical and Engineering Sciences **361**, 1349 (2003).

[39] We choose the two beams to have equal power, which gives the highest Raman Rabi rate at a fixed total power. Thus, this results in a simple factor of 2 coming from scattering off 2 beams.

[40] R. Wynar, R. S. Freeland, D. J. Han, C. Ryu, and D. J. Heinzen, Science **287**, 1016 (2000).

[41] T. Rom, T. Best, O. Mandel, A. Widera, M. Greiner, T. W. Hänsch, and I. Bloch, Phys. Rev. Lett. **93**, 073002 (2004).

[42] A. Grochola, P. Kowalczyk, J. Szczepkowski, W. Jastrzebski, A. Wakim, P. Zabawa, and N. P. Bigelow, Phys. Rev. A **84**, 012507 (2011).

[43] L. R. Liu, J. T. Zhang, Y. Yu, N. R. Hutzler, Y. Liu, T. Rosenband, and K.-K. Ni, arXiv:1701.03121 (2017).

[44] There is an additional factor of 2, with both beams at equal power, to account for the Stark shift caused by both beams.

[45] F. H. Mies, E. Tiesinga, and P. S. Julienne, Phys. Rev. A **61**, 022721 (2000).

[46] J. D. Hood, Y. Yu, Y.-W. Lin, J. T. Zhang, K. Wang, L. R. Liu, B. Gao, and K.-K. Ni, Phys. Rev. Research **2**, 023108 (2020).

[47] L. R. Liu, J. D. Hood, Y. Yu, J. T. Zhang, N. R. Hutzler, T. Rosenband, and K.-K. Ni, Science **360**, 900 (2018).

[48] L. R. Liu, J. D. Hood, Y. Yu, J. T. Zhang, K. Wang, Y.-W. Lin, T. Rosenband, and K.-K. Ni, Phys. Rev. X **9**, 021039 (2019).

[49] K. Wang, X. He, R. Guo, P. Xu, C. Sheng, J. Zhuang, Z. Xiong, M. Liu, J. Wang, and M. Zhan, Phys. Rev. A **100**, 063429 (2019).

[50] This interaction shift is larger than the differential axial trapping frequency between Na and Cs atoms, which decouples the relative and center of mass motional state and improves the robustness of our preparation of the relative motional ground state.

[51] D. Barredo, S. de Léséleuc, V. Lienhard, T. Lahaye, and A. Browaeys, Science **354**, 1021 (2016).

[52] M. Endres, H. Bernien, A. Keesling, H. Levine, E. R. Anschuetz, A. Krajenbrink, C. Senko, V. Vuletic, M. Greiner, and M. D. Lukin, Science **354**, 1024 (2016).